Antifungal and antimycobacterial activity of new N^1-[1-aryl-2-(1*H*-imidazol-1-yl and 1*H*-1,2,4-triazol-1-yl)-ethylidene]-pyridine-2-carboxamidrazone derivatives: a combined experimental and computational approach

Maria Grazia Mamolo,[a*] Daniele Zampieri,[a] Valeria Falagiani,[a] Luciano Vio,[a] Maurizio Fermeglia,[b] Marco Ferrone,[b] Sabrina Pricl,[b] Elena Banfi,[c] and Giuditta Scialino[c]

[a] *Department of Pharmaceutical Sciences, Piazzale Europa 1,University of Trieste, 34127 Trieste,Italy*

[b] *Department of Chemical, Environmental and Raw Materials Engineering, Piazzale Europa 1, University of Trieste, 34127 Trieste, Italy*

[c] *Department of Biomedical Sciences, Microbiology Section, Via A.Fleming 32, University of Trieste,34127 Trieste, Italy*

E–mail: mamolo@units.it

Dedicated to Professor Vincenzo Tortorella in the occasion of his "Fuori Ruolo" status

(received 17 Dec 03; accepted 17 Mar 04; published on the web 23 Mar 04)

Abstract

N^1-[1-Aryl-2-(1*H*-imidazol-1-yl and 1*H*-1,2,4-triazol-1-yl)-ethylidene]-pyridine-2-carboxamidrazone derivatives were synthesized and tested for their *in vitro* antifungal and antimycobacterial activity. Some compounds showed a very good activity against the tested clinical isolates of *Candida albicans* 685 and *Candida glabrata* 523. The same compounds exhibited an interesting, even if moderate, activity against the tested strain of *Mycobacterium tuberculosis* H_{37}Rv. Preliminary molecular modeling investigations yielded free energy of binding values in harmony with the corresponding experimental findings. They further revealed that an optimized balance of opposing electrostatic contributions must be realized to gain tight enzyme-inhibitor binding.

Keywords: *In vitro* antifungal and antimycobacterial activity, Preliminary molecular modeling investigations, N^1-pyridine-2-carboxamidrazone derivatives

Introduction

Considering the increased incidence of severe opportunistic fungal infections in immunocompromised patients together with the development of resistance among pathogenic

Candida spp., there is a great need for new antifungal compounds. On the other hand, the increase of tuberculosis due to emergence of multidrug-resistant strains of *Mycobacterium tuberculosis*, together with the increased incidence of severe disseminated infections produced by mycobacteria other than tuberculosis in immunocompromised patients, have prompted the search for new antimycobacterial drugs.

Because many imidazole derivatives showed potent antimycobacterial activity associated with good antifungal activity,[1,2] we synthesized a series of compounds **2 a-l** in which the 1-aryl-2-(1H-azol-1-yl)-ethane moiety, present in many azole antifungal drugs, is linked through a azomethine linkage to pyridine-2-carboxamidrazone, whose importance with respect to the antimycobacterial activity of a number of derivatives has been previously described.[3-9]

The *in vitro* activities of derivatives **2 a-l** were tested against two clinical strains of *Candida albicans* 685 and *Candida glabrata* 523 in comparison with miconazole and amphotericin B, and against a strain of *Mycobacterium tuberculosis* $H_{37}Rv$ in comparison with isoniazid and rifampicin. Since the synthesized compounds showed a remarkable antifungal activity, we present a preliminary study in order to verify how the synthesized azole compounds interact at the target enzyme cytocrome P450-dependent lanosterol 14a -demethylase ($P450_{14DM}$, CYP51) in the ergosterol-biosynthesis pathway. This study was performed through a preliminary computer modeling of drug/enzyme complexes in order to calculate relative free energies of association of these molecules, to relate these values to experiment, and to obtain mechanistic insight into binding modes and non covalent association. All these evidences can be of use in further experimental protein-ligand design.

Results and Discussion

All newly synthesized imidazole derivatives **2 a-e** and **2 k,l** showed antifungal activity after 24 and 48h towards the tested clinical strain of *Candida albicans* 685 (Table 1).

The most active compounds were the imidazole derivatives **2b** and **2c**, whose MIC values were 0.125 and 0.25 μg/ml after 24h and 48h. Compounds **2b** and **2c** were substituted on the *para* position of the phenyl ring with the electron-withdrawing bromo and chloro substituents, respectively. Their activities were superior than that of the reference drug amphotericyn B. The 4-phenyl substituted derivative **2e** retains a good activity level, with MIC values of 0.25 and 0.5 μg/ml.

The antifungal activities of the unsubstituted compound **2a** (MIC = 2 and 4 μg/ml) and of the compound **2d** (MIC = 0.5 and 4 μg/ml), *para*-substituted on the phenyl ring with the electron-donating methyl group, were rather inferior. The thienyl derivatives **2k** (MIC = 0.5 and 2 μg/ml) and **2l** (MIC = 0.5 and 2 μg/ml) substituted at the 5 position with bromine and chlorine, respectively, exhibited rather good activities, even if inferior than those of the corresponding *para*-bromophenyl and *para*-chlorophenyl derivatives **2b** and **2c**. However, with the exception of

the *para*-chloro substituted compound **2h**, none of the triazole derivatives **2f**, **g**, **i**, **j** showed antifungal activity towards the strain of *Candida albicans* 685 after 48h.

Table 1. Antifungal activity of compounds **2 a-l** (MIC = μg/ml) against two clinical isolates of *Candida* species

Comp.	C.albicans 685		Candida glabrata 523	
	After 24h	After 48h	After 24h	After 48h
2a	2	4	4	64
2b	0.125	0.25	0.5	1
2c	0.125	0.25	0.5	1
2d	0.5	4	4	32
2e	0.25	0.5	0.5	2
2f	64	64	64	64
2g	2	64	8	64
2h	2	8	8	64
2i	64	64	64	64
2j	64	64	64	64
2k	0.5	2	2	32
2l	0.5	2	2	32
AMB	1	1	1	2
Mic	0.078	0.078	1.25	1.25

The antifungal activities of compounds **2 a-l** against the tested strain of *Candida glabrata* 523 (Table 1) had a profile similar to their activities against the strain of *Candida albicans* 685. The most active compounds were the *para*-bromophenyl derivative **2b** (MIC = 0.5 and 1 μg/ml) and the *para*-chlorophenyl derivative **2c** (MIC = 0.5 and 1 μg/ml). Their activities were superior than those of the reference drugs amphotericyn B and miconazole. The unsubstituted derivative **2a** exhibited antifungal activity only after 24h (MIC = 4 μg/ml) whereas the 4-biphenylyl derivative **2e** showed a good activity after 24 and 48h (MIC = 0.5 and 2 μg/ml).

The presence of the electron-donating methyl group in the *para* position at the phenyl residue of compounds **2d** substantially decrease the antifungal activity (MIC = 4 and 32 μg/ml). All the triazole derivatives **2 f-j** were devoid of activity towards *Candida glabrata* 523 after 48h.

From the obtained data only compounds bearing an imidazole residue seems to be active against the tested microorganisms and substituents at the *para* position on the phenyl residue are able to modulate their activities. The replacement of the imidazole with the 1,2,4-triazole nucleus decreases or abolishes the antimicotic activities of the corresponding compounds. The presence

of the imidazole residue in the studied compounds appears to be essential for their activity whereas the 2-pyridinecarboxamidrazone moiety may furnish a contribution only to the activity of the imidazole derivatives.

Moreover, compounds **2 a-l** were tested against a strain of *Mycobacterium tuberculosis* $H_{37}Rv$. The imidazole derivatives **2 b,c** and **2e**, characterized by the presence of bromo, chloro and phenyl substituents, respectively, at the *para* position of the benzene ring, explicated (Table 2) a moderate antimycobacterial activity (MIC = 10 μg/ml), as did the corresponding 5-bromo and 5-chlorothienyl derivatives **2 k,l** (MIC = 10 μg/ml). Triazole derivatives **2 g,h,j** were weakly active (MIC = 40 μg/ml) whereas derivatives **2f** and **2i** were inactive. Accordingly to the results obtained for other imidazole derivatives[2,3], the newly synthesized imidazole derivatives **2 b-e** and **2 k,l** showed both *in vitro* antifungal and antimycobacterial properties.

Table 2. Activity of compounds **2a–l** against *M*. *tuberculosis* $H_{37}Rv$[(a)]

Comp.	MIC μg/ml	Comp.	MIC μg/ml
2a	40	**2g**	40
2b	10	**2h**	40
2c	10	**2i**	40
2d	20	**2j**	40
2e	10	**2k**	10
2f	40	**2l**	10

[(a)] *M*. *tuberculosis* $H_{37}Rv$ strain resulted sensitive to isoniazid (5 μg/disk) and rifampicin (30 μg/disk).

Chemistry

The synthesis of N^1-[1-aryl-2-(1*H*-imidazol-1-yl)-ethylidene]-pyridine-2-carboxamidrazone **2 a-e** and N^1-[1-aryl-2-(1*H*-1,2,4-triazol-1-yl)-ethylidene]-pyridine-2-carboxamidrazone derivatives **2 f-j** (Table 3) was carried out (Scheme 1) by treating the corresponding 1-aryl-2-(1*H*-imidazol-1-yl)-ethanone **1 a-e** and 1-aryl-2-(1*H*-1,2,4-triazol-1-yl)-ethanone **1f-j** derivatives with pyridine-2-carboxamidrazone. The intermediate ethanone derivatives **1a-j** were prepared from the substituted 2-bromoacetophenones and imidazole or triazole, according to the described procedure. The substituted N^1-[1-(thiophen-2-yl)-2-(1*H*-imidazol-1-yl)-ethylidene]-pyridine-2-carboxamidrazone derivatives **2 k,l** (Table 2) were similarly obtained (Scheme 1) by condensation of the corresponding ethanone intermediates **1 k,l** with pyridine-2-carboxamidrazone. The ethanone intermediate **1k** was not previously described.

Table 3. Yields and physical data of the synthesized compounds

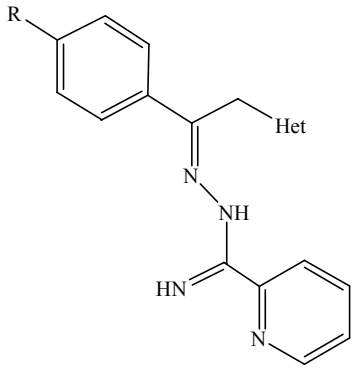

Comp.	R	Het	Yield (%)	M.p.(°C)	Formula
2a	H	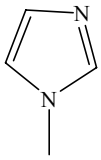	45.60	118-20	$C_{17}H_{16}N_6$
2b	Br		47.38	163-65	$C_{17}H_{15}N_6Br$
2c	Cl		48.96	168-172	$C_{17}H_{15}N_6Cl$
2d	CH_3		41.82	148-50	$C_{18}H_{18}N_6$
2e	Ph		45.31	163-65	$C_{23}H_{20}N_6$
2f	H	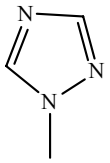	47.69	141-43	$C_{16}H_{15}N_7$
2g	Br		47.89	155-57	$C_{16}H_{14}N_7Br$
2h	Cl		51.51	145-47	$C_{16}H_{14}N_7Cl$
2i	CH_3		60.49	155-57	$C_{17}H_{17}N_7$
2j	Ph		60.80	175-77	$C_{22}H_{19}N_7$
2k	Br	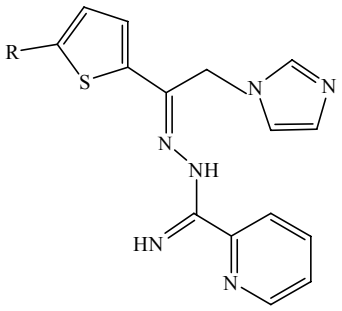	47.20	149-51	$C_{15}H_{13}N_6SBr$
2l	Cl		46.45	177-79	$C_{15}H_{13}N_6SCl \cdot HNO_3$

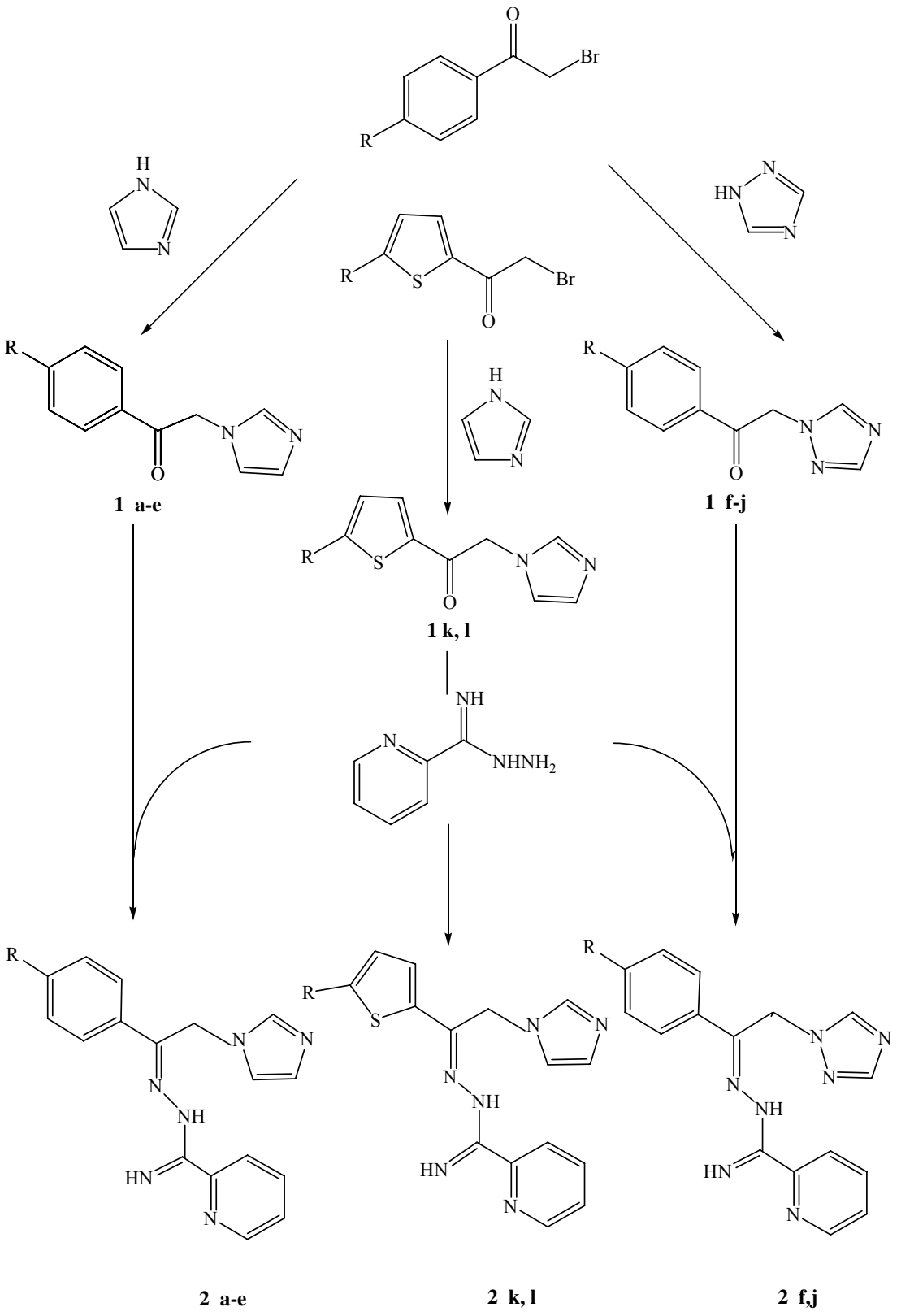

Scheme 1

Molecular modelling

According to the procedure adopted, all 12 azole compounds plus miconazole were characterized by a similar docking mode in the active site of the cytochrome P450 14a-sterol demethylase (14DM) from *Candida albicans*. The imidazole ring (**2a-e, 2k-l** and miconazole) or triazole ring (**2f-j**) is positioned almost perpendicular to the porphyrine plan, with a ring nitrogen atom coordinated to the heme iron. The analysis of the MD trajectories revealed that the average distance between N3(4) of the azole ring and the heme iron is 2.01 ± 0.4 Å, in good agreement with that found in the crystal structure of $P450_{cam}$ complexed with azole inhibitors.[10]

The phenyl group of compounds **2a-j** and one aromatic ring of miconazole, as well as the thienyl moiety of **2k-l**, locates in a hydrophobic binding cleft, above the heme ring. This subsite includes the side chains of the ceiling residues F186, P187, H261, V460 and V461. The larger size of the phenyl ring extends the number of contacts in the binding site in comparison with those established by compounds characterized by the presence of the smaller thienyl ring. The pyridine ring, common to all inhibitors, and the other, halogenated phenyl ring of miconazole, is stabilized by favorable dispersion forces with the side chains of K98, L354, V355, P357 and Y359. Further stabilizing nonbonded interactions are established between the azole ring of the inhibitors and residues G254, M257, G258 and T262. As an example, Figure 1 (a), (b), (c) and (d) shows the resulting molecular models of the docked **2c**/ **2h**/, **2l**/ and miconazole/14DM complexes, respectively.

Further insights into the forces involved in substrate binding can be obtained by analyzing the free energy components, which are listed in Tables 4 to 6 for all the ligands. Table 4 also reports the values obtained for miconazole for comparison. As we may see from these Tables, both the intermolecular van der Waals and the electrostatics are important contributions to the binding.

Table 4. Energy terms and total free energy of binding (kcal/mol) between 14DM and compounds **2a-e**, and between 14DM and miconazole

	2a	**2b**	**2c**	**2d**	**2e**	**Mic**
ΔE_{MM}^{ele}	– 125.8	– 138.8	– 133.4	– 125.9	– 123.6	– 175.9
ΔE_{MM}^{vdW}	– 42.0	– 41.1	– 44.3	– 41.8	– 40.8	– 49.1
ΔE_{MM}	– 167.8	– 179.9	– 177.7	– 167.7	– 164.4	– 225.0
ΔG_{sol}^{np}	– 2.9	– 3.0	– 2.9	– 2.9	– 3.3	– 3.4
ΔG_{sol}^{ele}	160.1	168.5	163.9	159.2	154.2	207.7
ΔG_{sol}	157.2	165.5	161.0	156.3	150.9	204.3
ΔG_{tot}^{ele}	31.4	26.7	27.6	30.4	27.3	28.4
ΔG_{bind}	– 10.6	– 14.4	– 16.7	– 11.4	– 13.5	– 20.1

Table 5. Energy terms and total free energy of binding (kcal/mol) of 14DM and compounds **2f-j**

	2f	**2g**	**2h**	**2i**	**2j**
ΔE_{MM}^{ele}	– 44.1	– 48.7	– 46.4	– 40.8	– 37.1
ΔE_{MM}^{vdW}	– 37.5	– 38.5	– 39.2	– 39.8	– 38.2
ΔE_{MM}	– 81.6	– 87.2	– 85.6	– 80.6	– 75.3
ΔG_{sol}^{np}	– 2.8	– 2.9	– 2.9	– 2.9	– 3.1
ΔG_{sol}^{ele}	80.2	85.5	83.6	79.1	73.2
ΔG_{sol}	77.4	82.6	80.7	75.2	70.1
ΔG_{tot}^{ele}	33.3	33.9	34.3	34.4	33.0
ΔG_{bind}	– 4.3	– 4.6	– 4.9	– 5.4	– 5.2

Table 6. Energy terms and total free energy of binding (kcal/mol) of 14DM and compounds **2k-l**

	2k	**2l**
ΔE_{MM}^{ele}	– 122.0	– 123.1
ΔE_{MM}^{vdW}	– 40.6	– 39.6
ΔE_{MM}	– 162.6	– 162.7
ΔG_{sol}^{np}	– 2.9	– 2.9
ΔG_{sol}^{ele}	153.5	152.8
ΔG_{sol}	150.6	149.9
ΔG_{tot}^{ele}	28.6	26.8
ΔG_{bind}	– 12.0	– 12.8

Comparing the van der Waals/non polar ($\Delta E_{MM}^{vdW} + \Delta G_{sol}^{np}$) with the electrostatic ($\Delta E_{MM}^{ele} + \Delta G_{sol}^{ele}$) contributions for all molecules, however, we see that in all cases the association between inhibitors and the target protein is mainly driven by more favorable nonpolar interactions in the complex than in solution. Those nonelectrostatic components are very similar for all series of compounds considered (ranging from approximately -42 to -47 kcal/mol). When examining the role of the electrostatics in the inhibitor-enzyme complex formation, however, it is fundamental to consider the electrostatic component of the molecular mechanical energy ΔG_{int}^{ele} together with the electrostatic contribution to solvation ΔG_{sol}^{ele}.

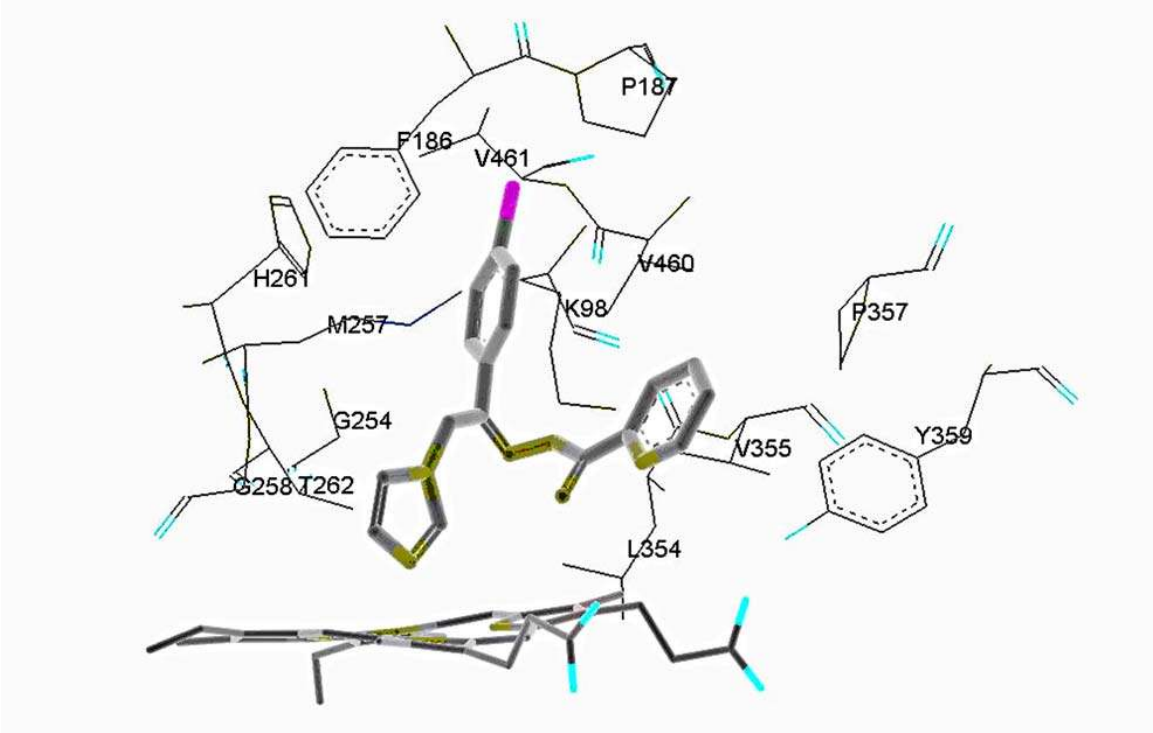

Figure 1a

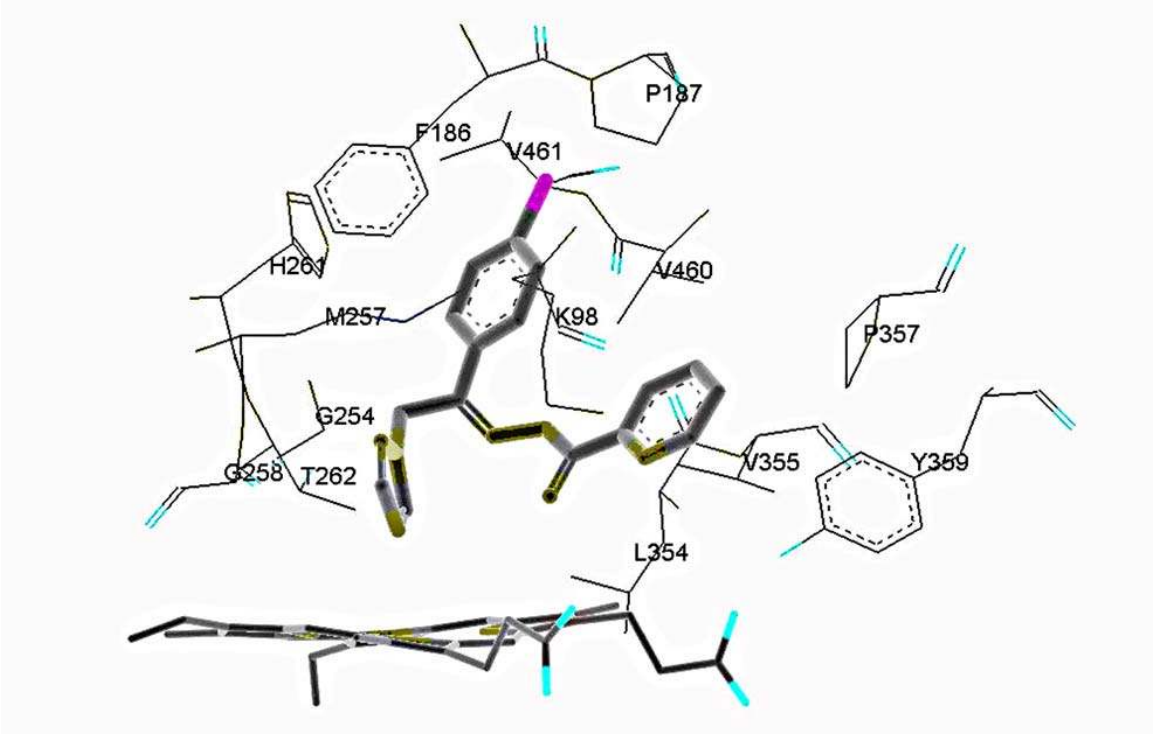

Figure 1b

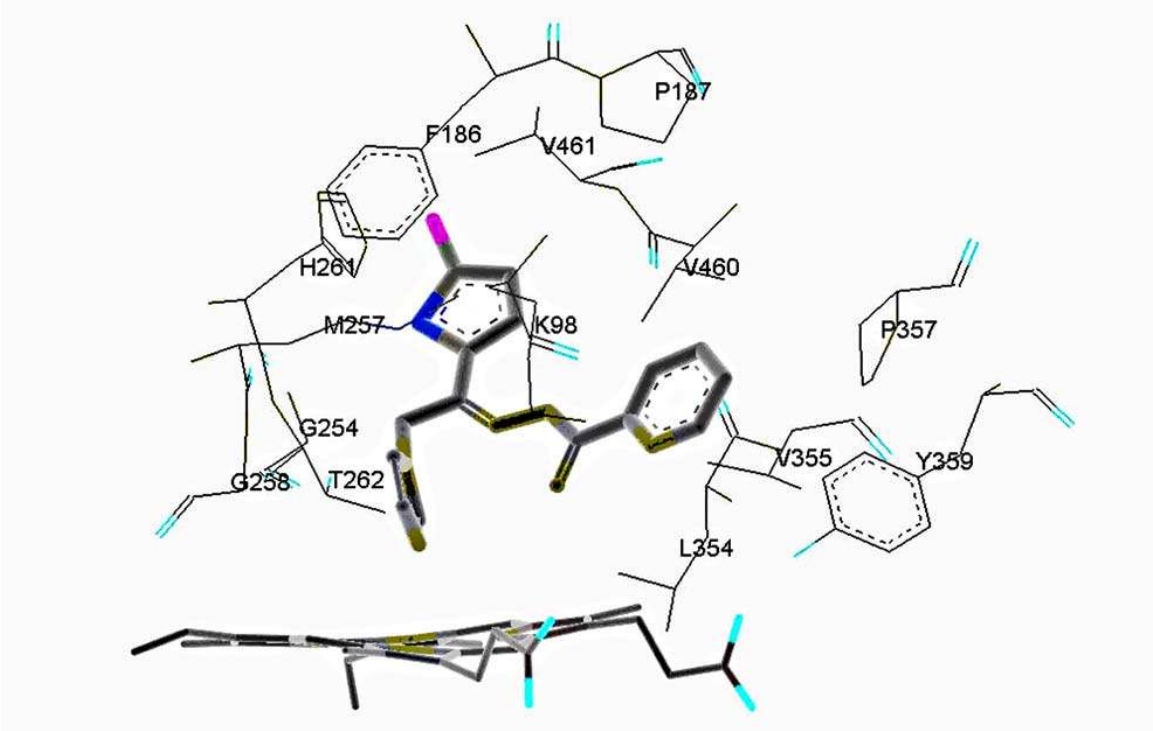

Figure 1c

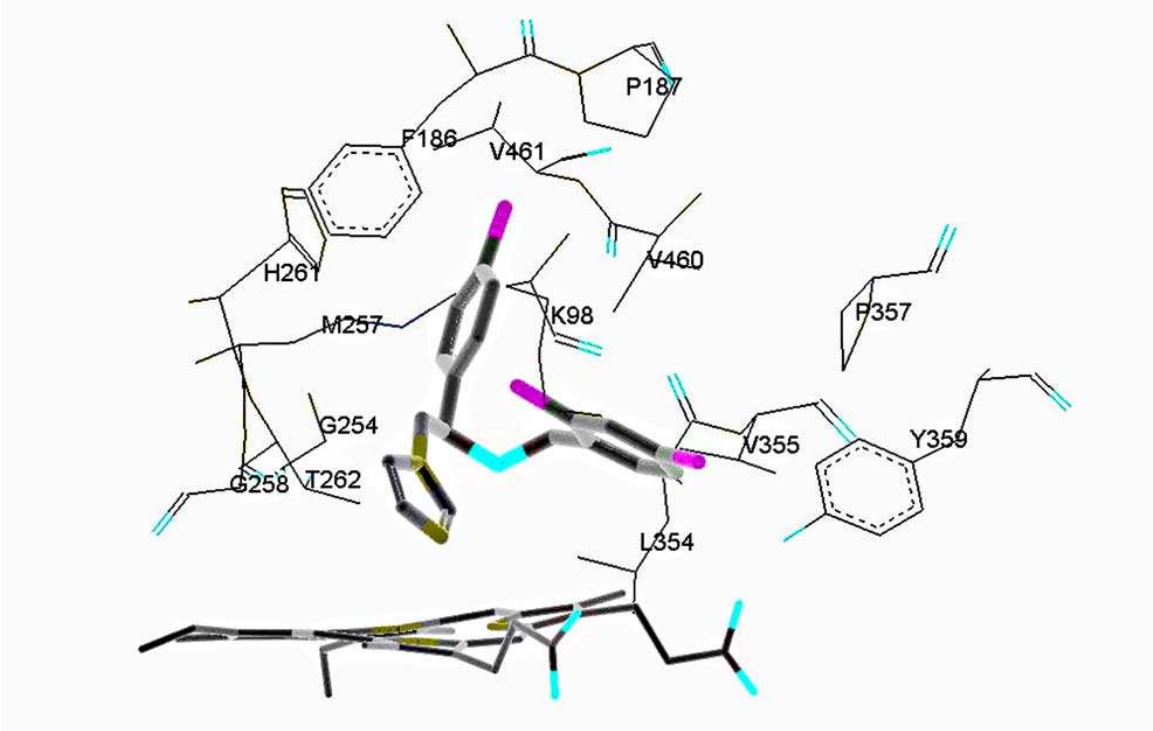

Figure 1d

As demonstrated by numerous studies,[11-17] electrostatics generally disfavor the docking of ligand and receptor molecules because of the unfavorable change in the electrostatics of solvation is mostly, but not fully, compensated by the favorable electrostatics within the resulting ligand-receptor complex. Indeed, the total electrostatic energy contributions (ΔG^{ele}_{tot} values) for all 14DM/azole derivative complex formations are unfavorable, the **2a-e**/14DM, the **2k-l**/14DM and the miconazole/14DM complex formations being less unfavorable than the **2f-j**/14DM complex formations because of a less positive total electrostatic term in which the penalty paid by the electrostatics of solvation is better compensated by favorable electrostatic interactions within the complex. Thus, even though electrostatics destabilize azole derivative/14DM complex formation, it is the optimized balance of opposing electrostatic contributions that leads to tighter binding both in the case of the reference compound miconazole, and in the series of compounds **2a-e** and **2k-l**.

Molecular dynamics simulations have thus shown to be able to rank binding affinities of all inhibitors, and to provide insight into the interactions occurring in the active site and the origins of variations in the corresponding binding free energy. Accordingly, the computational strategy used in this paper can provide a blueprint for new inhibitors in structure-based drug design or in predicting binding affinity of a ligand prior to organic synthesis.

Experimental Section

General Procedures. Melting points were determined with a Büchi 510 capillary apparatus, and are uncorrected. Infrared spectra in nujol mulls were recorded on a Jasco FT 200 spectrophotometer. Proton nuclear magnetic resonance (1H-NMR) spectra were determined on a Varian Gemini 200 spectrometer; chemical shifts are reported as δ (ppm) in $DMSOd_6$ solution. Reaction courses and product mixtures were routinely monitored by thin-layer chromatography (TLC) on silica gel precoated F254 Merck plates. ESI-MS spectra were obtained on a PE-API 1 spectrometer by infusion of a solution of the sample in MeOH. Elemental analyses (C, H, N) were performed on a Carlo Erba analyzer and were within ± 0.3 of the theoretical value.

Synthesis

1-(5-Bromo-thiophen-2-yl)-2-(1*H*-imidazol-1-yl)-ethanone (1k)

To a solution of 1.5 g (5.3 mmol) of 2-bromo-1-(5-bromo-thiophen-2-yl)-ethanone in 30 ml of tetrahydrofuran, 1.1 g (15.9 mmol) of imidazole were added under stirring. The reaction mixture was stirred at room temperature for 12 h. Thereafter, the solvent was removed under reduced pressure. The solid residue was dissolved in dichloromethane and the solution was washed with cold water, dried (Na_2SO_4) and filtered. The filtrate was evaporated to dryness to give a residue which was recrystallized from ethanol to give 1.3 g (83 %) of **1k**; m. p. 158-160°C.

IR (nujol, cm^{-1}): 1668. ^{1}H-NMR (DMSO-d_6/TMS): δ 5.58 (s, 2H, CH_2), 6.89 (s, 1H, imid.), 7.10 (s, 1H, imid.), 7.45 (d, 1H, thioph.; J=3.66 Hz), 7.58 (s, 1H, imid.), 7.92 (d, 1H, thioph. J=

3.66 Hz). MS: m/z 271 [MH^+], 273 [MH^++2]. Anal. calcd for $C_9H_7N_2BrOS$ (MW 271.13): C, 39.87; H, 2.60; N, 10.33%; found: C, 39.72; H, 2.48; N, 10.47%.

***N*^{1}-[1-Phenyl-2-(1*H*-imidazol-1-yl)-ethylidene]-pyridine-2-carboxamidrazone (2a).** A solution of 1 g (5.4 mmol) of 2-(1*H*-imidazol-1-yl)-1-phenyl-ethanone, **1a**, in 30 ml of absolute ethanol, was treated with few drops of acetic acid. To stirred solution 0.73 g (5.4 mmol) of 2-pyridinecarboxamidrazone in 10 ml of absolute ethanol were added dropwise and the reaction mixture was heated at the reflux for 6 h. Thereafter, the solvent was completely evaporated under reduced pressure and the solid residue was washed with distilled water, collected by filtration and recrystallized from absolute ethanol to obtain 0.9 g (71 %) of **2a**; m. p. 119-121°C.

IR (nujol, cm^{-1}): 3100, 3445. ^{1}H-NMR ($CDCl_3$/TMS): δ 5.56 (br. s, 2H, CH_2), 6.46 (s, 1H, NH, disappearing on deuteration), 6.80 (br. s, 1H, NH, disappearing on deuteration), 6.95-6.99 (m, 2H, imid.), 7.35-7.40 (m, 4H, 1H pyr., 3H arom.), 7.61 (s, 1H, imid.), 7.72-7.84 (m, 3H, 1H pyr., 2H arom.), 8.32 (m, 1H, pyr.), 8.59 (m, 1H, pyr.). MS: m/z 304 [M^+]. Anal. calcd for $C_{16}H_{15}N_6$ (MW 304.35): C, 67.09; H, 5.30; N, 27.61%; found: C, 67.35; H, 5.47; N, 27.48%.

In an analogous way the following compounds **2b-k** have been prepared. Yields and melting points are reported in Table 1.

***N*^{1}-[1-(4-Bromophenyl)-2-(1*H*-imidazol-1-yl)-ethylidene]-pyridine-2-carboxamidrazone (2b).** IR (nujol, cm^{-1}): 3170, 3407. ^{1}H-NMR ($CDCl_3$-TMS) δ: 5.52 (s, 2H, CH_2), 6.43 (br.s. 1H, NH, disappearing on deuteration), 6.87 (br.s, 1H, NH, disappearing on deuteration), 6.96 (m, 2H, imid.), 7.35-7.82 (m, 5H, 2H pyr., 4H arom., 1H imid), 8.30 (m,1H, pyr.), 8.60 (m, 1H, pyr.). MS: 383 m/z [MH^+], 385 [MH^++2]. Anal. calcd for $C_{17}H_{15}N_6Br$ (MW 383.25): C, 53.28; H, 3.95; N, 21.93%; found: C, 53.39; H, 3.74; N, 22.19%.

***N*^{1}-[1-(4-Chlorophenyl)-2-(1*H*-imidazol-1-yl)-ethylidene]-pyridine-2-carboxamidrazone (2c).** IR (nujol, cm^{-1}): 3140, 3405. ^{1}H-NMR ($CHCl_3$-TMS) δ: 5.52 (s, 2H, CH_2), 6.45 (br.s, 1H, NH, disappearing on deuteration), 6.86 (br.s, 1H, NH, disappearing on deuteration), 6.95 (m, 2H, imid.), 7.24-7.79 (m, 7H, 2H pyr., 4H arom., 1H imid.), 8.30 (m, 1H, pyr.), 8.59 (m, 1H, pyr.). MS: m/z 339 [MH^+], 341 [MH^++2]. Anal. calcd for $C_{17}H_{15}N_6Cl$ (MW 338.79): C, 60.27; H, 4.46; N, 24.81%; found: C, 60.41; H, 4.28; N, 24.96%.

***N*^{1}-[1-(4-Methylphenyl)-2-(1*H*-imidazol-1-yl)-ethylidene]-pyridine-2-carboxamidrazone (2d).** IR (nujol, cm^{-1}): 3172, 3464. ^{1}H-NMR ($CDCl_3$-TMS) δ: 2.37 (s, 3H, CH_3), 5.57 (s, 2H, CH_2), 6.49 (br.s., 1H, NH, disappearing on deuteration), 6.77 (br.s., 1H, NH, disappearing on deuteration), 6.99 (m, 2H, imid.), 7.17-7.42 (m, 3H, 1H pyr., 2H arom.), 7.63-7.84 (m, 3H, 1H pyr., 1H imid., 2H arom.), 8.34 (m, 1H, pyr.), 8.61 (m, 1H, pyr.). MS: m/z 319 [MH^+]. Anal. calcd for $C_{18}H_{18}N_6$ (MW 318.38): C, 67.90; H, 5.70; N, 26.40%; found: C, 68.12; H, 5.57; N, 26.41%.

***N*^{1}-[1-(Biphenyl-4-yl)-2-(1*H*-imidazol-1-yl)-ethylidene]-pyridine-2-carboxamidrazone (2e).** IR (nujol, cm^{-1}): 3289, 3445. ^{1}H-NMR ($CDCl_3$-TMS) δ: 5.57 (s, 2H, CH_2), 6.50 (br.s., 1H, NH, disappearing on deuteration), 6.86 (br.s., 1H, NH, disappearing on deuteration), 6.99 (m, 2H, imid.), 7.24- 7.92 (m, 12H, 9H arom., 2H pyr., 1H imid.), 8.34 (m, 1H, pyr.), 8.59 (m, 1H, pyr.).

MS: m/z 381 [MH^+]. Anal. calcd for $C_{23}H_{20}N_6$ (MW 380.45): C, 72.61; H, 5.30; N, 22.09%; found: C, 72.78; H, 5.24; N, 22.23%.

***N*^{1}-[1-Phenyl-2-(1*H*-1,2,4-triazol-1-yl)-ethylidene]-pyridine-2-carboxamidrazone (2f).** IR (nujol, cm^{-1}): 3433, 3319. ^{1}H-NMR ($CDCl_3$-TMS) δ: 5.83 (s, 2H, CH_2), 6.43 (br.s., 1H, NH disappearing on deuteration), 6.83 (br.s., 1H, NH disappearing on deuteration), 7.37-7.49 (m, 4H, 1H pyr., 3H arom.), 7.74-8.0 (m, 4H, 1H pyr., 1H triaz., 2H arom.), 8.23- 8.34 (m, 2H, 1H pyr, 1H triaz.), 8.61 (m, 1H, pyr.). MS: m/z 306 [MH^+]. Anal. calcd for $C_{16}H_{15}N_7$ (MW 305.34): C, 62.94; H, 4.95; N, 32.11%; found: C, 62.78; H, 5.12; N, 32.29%.

***N*^{1}-[1-(4-Bromophenyl)-2-(1*H*-1,2,4-triazol-1-yl)-ethylidene]-pyridine-2-carboxamidrazone (2g).** IR (nujol, cm^{-1}): 3336, 3461. ^{1}H-NMR ($CDCl_3$-TMS) δ: 5.77 (s, 2H, CH_2), 6.39 (br.s., 1H, NH disappearing on deuteration), 6.87 (br.s., 1H, NH disappearing on deuteration), 7.33-7.57 (m, 3H, 1H pyr., 2H arom.), 7.65-7.95 (m, 4H, 1H pyr., 1H triaz., 2H arom.), 8.21-8.33 (m, 2H, 1H triaz., 1H pyr.), 8.61 (m, 1H, pyr). MS: m/z 384 [MH^+], 386 [MH^++2]. Anal. calcd for $C_{16}H_{14}N_7Br$ (MW 384.23): C, 50.01; H, 3.67; N, 25.52%; found: C, 50.16; H, 3.43; N, 25.77%.

***N*^{1}-[1-(4-Chlorophenyl)-2-(1*H*-1,2,4-triazol-1-yl)-ethylidene]-pyridine-2-carboxamidrazone (2h).** IR (nujol, cm^{-1}): 3329, 3440. ^{1}H-NMR ($CDCl_3$-TMS) δ: 5.77(s, 2H, CH_2), 6.43 (br.s., 1H, NH, disappearing on deuteration), 6.90 (br.s., 1H, NH, disappearing on deuteration), 7.33-7.43 (m, 3H, 1H pyr., 2H arom.), 7.74-7.95 (m, 4H, 1H pyr., 2H arom., 1H triaz.), 8.23-8.33 (m, 2H, 1H pyr., 1H triaz.), 8.60 (m, 1H, pyr.). MS: m/z 340 [MH^+], 342 [MH^++2]. Anal. calcd for $C_{16}H_{14}N_7Cl$ (MW 339.78): C, 56.56; H, 4.15; N, 28.86%; found: C, 56.78; H, 4.32; N, 28.63%.

***N*^{1}-[1-(4-Methylphenyl)-2-(1*H*-1,2,4-triazol-1-yl)-ethylidene]-pyridine-2-carboxamidrazone (2i).** IR (nujol, cm^{-1}): 3339, 3459. ^{1}H-NMR ($CDCl_3$-TMS) δ: 2.35 (s, 3H, CH_3), 5.79 (s, 2H, CH_2), 6.43 (br.s., 1H, NH disappearing on deuteration), 6.82 (br.s., 1H, NH disappearing on deuteration), 7.16-7.24 (m, 2H, arom.), 7.37 (m, 1H, pyr.), 7.77 (m, 1H, pyr.), 7.86-7.90 (m, 3H, 2H arom., 1H triaz.), 8.21 (s, 1H, triaz.), 8.30 (m, 1H, pyr.), 8.59 (m, 1H, pyr.). MS: m/z 320 [MH^+]. Anal. calcd for $C_{17}H_{17}N_7$ (MW 319.36): C, 63.93; H, 5.37; N, 30.70%; found: C, 64.09; H, 5.22; N, 30.88%.

***N*^{1}-[1-(Biphenyl-4-yl)-2-(1*H*-1,2,4-triazol-1-yl)-ethylidene]-pyridine-2-carboxamidrazone (2j).** IR (nujol, cm^{-1}): 3450, 3320. ^{1}H-NMR ($CDCl_3$-TMS) δ: 5.84 (s, 2H, CH_2), 6.51 (br.s., 1H, NH disappearing on deuteration), 6.88 (br.s., 1H, NH disappearing on deuteration), 7.35-7.48 (m, 4H, 1H pyr., 3H arom.), 7.58-7.91 (m, 6H, 1H pyr., 1H triaz., 4H arom.), 8.07-8.10 (m, 2H, arom.), 8.27- 8.35 (m, 2H, 1H pyr., 1H triaz.), 8.61 (m, 1H, pyr.). MS: m/z 382 [MH^+]. Anal. calcd for $C_{22}H_{19}N_7$ (MW 381.43): C, 69.27; H, 5.02; N, 25.70%; found: C, 69.31; H, 5.12; N, 25.58%.

***N*^{1}-[1-(5-Bromo-thiophen-2-yl)-2-(1*H*-imidazol-1-yl)-ethylidene]-pyridine-2-carboxamidrazone (2k).** IR (nujol, cm^{-1}): 3330, 3450. ^{1}H-NMR (DMSO-d_6-TMS) δ: 5.51 (s, 2H, CH_2), 6.80 (s, 1H, imid.), 6.94 (br.s., 1H, NH, disappearing on deuteration), 7.14 (s, 1H, imid.), 7.22 (d, 1H, thioph., J=3.66 Hz), 7.38 (br.s., 1H, NH, disappearing on deuteration), 7.47-7.63 (m, 2H, 1H, pyr. and 1H thioph., J=3.66 Hz), 7.66 (s. 1H, imid.), 7.94 (m, 1H, pyr.), 8.36 (m, 1H, pyr.), 8.66

(m, 1H, pyr.). MS: m/z 389 [MH^+], 391 [MH^++2]. Anal. calcd for $C_{15}H_{13}N_6SBr$ (MW 389.27): C, 46.28; H, 3.37; N, 21.59%; found: C, 46.37; H, 3.19; N, 21.46%.

***N*^{1}-[1-(5-Chlorothiophen-2-yl)-2-(1*H*-imidazol-1-yl)-ethylidene]-pyridine-2-carboxamidrazo-ne nitrate (2l). This compound was prepared starting from 1-(5-chloro-thiophen-2-yl)-2-(1H-imidazol-1-yl)-ethanone nitrate[18].** IR (nujol, cm^{-1}): 3348, 3331. ^{1}H-NMR (DMSO-d_6-TMS) δ: 2.82-3.71 (br.s., 1H, NH^+, disappearing on deuteration), 5.66 (s, 2H, CH_2) 6.87 (br.s, 1H, NH, disappearing on deuteration), 7.23 (d, 1H, thioph. J=3.91 Hz) 7.52-7.65 (m, 2H, 1H pyr.; 1H, NH disappearing on deuteration), 7.65-7.76 (m, 2H, 1H imid.; 1H, thioph., J=3.91 Hz), 7.89 (s, 1H, imid.), 8.06 (m, 1H, pyr.), 8.31 (m, 1H, pyr.), 8.67 (m, 1H, pyr.), 9.32 (m, 1H, imid.). MS: m/z 345 [MH^+], 347 [MH^++2]. Anal. calcd for $C_{15}H_{13}N_6SCl{\cdot}HNO_3$ (MW 407.06): C, 44.17; H, 3.46; N, 24.04%; found: C, 44.32; H, 3.53; N, 23.96%.

Microbiology

The antimycobacterial activity has been evaluated on *Mycobacterium tuberculosis* reference strain H_{37}Rv. The inhibiting activity of the new molecules was tested by means of a standard agar dilution technique [19] with viable counts performed in quadrant petri plates containing Middlebrook and Cohn 7H11 agar, supplemented with Middlebrook OADC enrichment. Serial dimethylsulfoxide twofold dilutions of the different chemicals tested were placed in each quadrant; control plates were included with known antitubercular drugs and no drug. A 20 µl sample of each reference strain suspension, containing 10^4/ml mycobacteria in sterile saline with the addition of 0.02% polysorbate 80, was inoculated onto each chemical containing quadrant. All plates were incubated at 37°C in 5% CO_2 for 3-4 weeks. Minimal inhibiting concentration (MIC) of each compound was defined as the lowest chemical dilution associated with at least a 99% reduction in the number of visible colonies.

Two clinical isolates of *Candida* species were selected for testing the new compounds, including *C.glabrata* 523, *C.albicans* 685.

The susceptibility of the *Candida spp* isolates to the newly synthesised compounds was determined by means of the agar dilution technique, according to the raccomendations of the National Comitee for Clinical Laboratory Standards (NCCLS, 1995). Stock solutions of chemicals were prepared in DMSO at a concentration of 4 mg/ml; MICs were determined in Sabouraud quadrant agar plates containing serial twofold dilutions of the tested compounds; 20 µl inoculum of each fungal strain, containing 1-5 x 10^2 cells/ml was added onto agar surface; controls were performed without chemicals and with reference antifungal drugs (miconazole (Mic), amphotericin B (AMB)). All the plates were then placed at 35°C and read after 24h and 48h incubation.

Molecular modeling

The starting 3D model of cytochrome P450 14α-sterol demethylase (14DM) from *Candida albicans* was originally developed by Boscott and Grant,[20] and subsequently used by Kelly et al.[21] Hydrogens were added to the protein backbone and side chains with the PARSE module of

the AMBER 6.0 package.[22, 23] All ionizable residues were considered in the standard ionization state at neutral pH. The all-atom force field (FF) parameters by Cornell et al.[24] (in parm94.dat file of the AMBER 6.0 code) was applied for protein relaxation. The primary cut-off distance for nonbonded interaction was set to 12 Å, the cut-off taper for the Coulomb and van der Waals interactions were 1.2 and 2, respectively. The GB/SA continuum solvation model[25, 26] was used to mimic a water environment. Geometry refinement was carried out using the SANDER module via a combined steepest descent – conjugate gradient algorithm, using as a convergence criterion for the energy gradient the root-mean-square of the Cartesian elements of the gradient equal to 0.01 kcal/(mol Å). As expected, no relevant structural changes were observed between the active site of the 14DM relaxed structure and the original 3-D structure.

The model structures of compounds **2a-l**, and the structure of miconazole as a blank test, were generated using the 3-D sketcher tool of Materials Studio.[27] All the molecules were subjected to an initial energy minimization using Discover.[28] In this case, the convergence criterion was set to 10^{-4} kcal/(mol Å). The conformational search was carried out using a combined molecular mechanics/molecular dynamics simulated annealing (MDSA) protocol[29]. Accordingly, the relaxed structures were subjected to 5 repeated temperature cycles (from 298 K to 1000 K and back) using constant volume/constant temperature (NVT) MD conditions. At the end of each annealing cycle, the structures were again energy minimized to converge below 10^{-4} kcal/(mol Å), and only the structures corresponding to the minimum energy were used for further modeling. The electrostatic charges for the geometrically optimized azole derivatives were obtained by RESP,[24, 30-32] and the electrostatic potentials were produced by single-point quantum mechanical calculations at the Hartree-Fock level with a 6-31+G* basis set.[33]

The optimized structures of the antifungal compounds were docked into the 14DM active site according to a validated procedure.[34] To proceed with docking simulation, all non-polar hydrogen atoms of the small organic molecules were deleted, and their charges were automatically added to those of the corresponding carbon atom by the program AutoTors included in the suite AutoDock 3.0.[35] The relevant grids of affinity potentials used by AutoDock were calculated by running the program AutoGrid. In order to encase a reasonable region of the protein surface and interior volume, centered on the crystallographic identified binding site, the grids were 60 Å on each side. Grid spacing (0.375 Å), and 120 grid points were applied in each Cartesian direction so as to calculate mass-centered grid maps. Amber 12-6 and 12-10 Lennard-Jones parameters were used in modeling van der Waals interactions and hydrogen bonding (N-H, O-H and S-H), respectively. In the generation of the electrostatic grid maps, the distance dependent relative permittivity of Mehler and Solmajer[36] was applied.

For the docking of each compound to the protein, three hundred Monte Carlo/Simulated Annealing (MC/SA) runs were performed, with 100 constant temperature cycles for simulated annealing. Translation, quaternion parameters and torsions were set at random before SA runs. Each cycle had a maximum of 20,000 accepted or rejected moves, the minimal energy structure being passed to the next cycle. The temperature was reduced by a 0.95 factor per cycle from an initial value of RT = 100 cal/mol. For these calculations, the GB/SA implicit water model[25, 26]

was again used to mimic the solvated environment. The rotation of the angles Φ and Φ, and the angles of side chains were set free during the calculations. All other parameters of the MC/SA algorithm were kept as default. Following the docking procedure, all structures of compounds **2a-l** plus miconazole were subjected to cluster analysis with a tolerance of 1 Å for an all-atom root-mean-square (RMS) deviation from a lower-energy structure representing each cluster family. The structure of each resulting complex, in which the azole ring of the drug coordinated to the heme iron atom, and characterized by the lowest interaction energy, was selected for further evaluation.

Each best substrate/14DM complex resulting from the automated docking procedure was further refined in the AMBER suite using the quenched molecular dynamics method (QMD). In this case, 100 ps MD simulation at 298 K were employed to sample the conformational space of the substrate-enzyme complex in the GB/SA continuum solvation environment.[25, 26] The integration step was equal to 1 fs. After each ps, the system was cooled to 0 K, the structure was extensively minimized, and stored. To prevent global conformational changes of the enzyme, the backbone of the protein binding site were constrained by a harmonic force constant of 100 kcal/Å, whereas the amino acid side chains and the ligands were allowed moving without any constraint.

The best energy configuration of each complex resulting from the previous step was solvated by adding a sphere of TIP3P water molecules[37] with a 20 Å radius from the heme iron atom with the use of the cap option of the LEAP module of AMBER 6.0. The protein complex was neutralized adding a suitable number of counterions (Na^+ and Cl^-) in the positions of largest electrostatic potential, as determined by the module CION of the AMBER 6.0 platform. The counterions, which had distances larger than 16 Å from the active site, were fixed in space during all simulations to avoid artifactual long range electrostatic effects on the calculated free energies. After energy minimization of the water molecules for 1500 steps, and MD equilibration of the water sphere with fixed solute for 20 ps, further unfavorable interactions within the structures were relieved by progressively smaller positional restraints on the solute (from 25 to 0 kcal/(mol $Å^2$) for a total of 4000 steps. Each system was gradually heated to 298 K in three intervals, allowing a 5 ps interval per each 100 K, and then equilibrated for 50 ps at 298 K, followed by 400 ps of data collection runs, necessary for the estimation of the free energy of binding (*vide infra*). After the first 20 ps of MD equilibration, additional TIP3P water molecules were added to the 20 Å water cap to compensate for those who were able to diffuse into gaps of the enzyme. The MD simulations were performed at constant T = 298 K using the Berendsen coupling algorithm,[38] an integration time step of 1 fs, and the applications of the SHAKE algorithm[39] to constrain all bonds to their equilibrium values, thus removing high frequency vibrations. Long-range nonbonded interactions were truncated by using a 20 Å residue-based cut-off.

For the calculation of the binding free energy between 14DM and compounds **2a-l** in water, a total of 400 snapshots were saved during the MD data collection period described above, one snapshot per each 1 ps of MD simulation. The binding free energy ΔG_{bind} of each complex in

water was calculated according to the procedure proposed by Srinivasan et al.[40] According to this method, ΔG_{bind} is calculated as:

$$\Delta G_{bind} = \Delta E_{MM} + \Delta G^{C}_{sol} - \Delta G^{L}_{sol} - \Delta G^{P}_{sol} - T\Delta S \quad (1)$$

where ΔE_{MM} is the interaction energy between the ligand and the protein, ΔG^{C}_{sol}, ΔG^{L}_{sol} and ΔG^{P}_{sol} are the solvation free energy for the complex, the ligand and the protein, respectively, and $-T\Delta S$ is the conformational entropy contribution to the binding. All energetic analysis was done for only a single MD trajectory of the lactam/protein complex considered, with unbound protein and substrate snapshots taken from the snapshots of that trajectory.

ΔE_{MM} can be obtained from the molecular mechanics (MM) interaction energies as:

$$\Delta E_{MM} = \Delta E^{ele}_{MM} + \Delta E^{vdW}_{MM} \quad (2)$$

where ΔE^{ele}_{MM} and ΔE^{vdW}_{MM} are the electrostatic and van der Waals contributions to the interaction energy between the ligand and the receptor. We must point out here that the molecular mechanics energy ΔE_{MM} in Eq. (2) effectively consists also of a valence part, ΔE^{val}_{MM}, but, as the structure of the protein in its bound and unbound state is the same, the contribution of this term to the binding free energy is zero. Accordingly, this term has been omitted in Eq. (1). In our case, all other quantities were calculated with the ANAL and CARNAL modules from the AMBER 6.0 suite. The infinite cutoffs for all interactions and the parm94 force field parameters[24] were applied. The total solvation energy, ΔG_{sol}, is divided in two parts: the electrostatic contribution, ΔG^{ele}_{sol}, and the non-polar term, ΔG^{np}_{sol}:

$$\Delta G_{sol} = \Delta G^{ele}_{sol} + \Delta G^{np}_{sol} \quad (3)$$

The polar component of ΔG_{sol} was evaluated with the PB approach.[41] This procedure involves using a continuum solvent model, which represents the solute as a low dielectric medium (i.e. of dielectric constant $\varepsilon = 1$) with embedded charges and the solvent as a high dielectric medium ($\varepsilon = 80$) with no salt. All atomic charges were taken from the Cornell et al. force field,[24] since these are consistent with the MM energy calculations. However, as suggested by Chong et al.,[42] the atomic radii were taken from the PARSE parameter set[43] instead of the parm94 FF set because of the small size of hydrogens in the latter. The dielectric boundary is the contact surface between the radii of the solute and the radius (1.4 Å) of a water molecule. The numerical solution of the linearized Poisson-Boltzmann equations were solved on a cubic lattice by using the iterative finite-difference method implemented in the *DelPhi* software package.[44] The grid size used was 0.5 Å. Potentials at the boundaries of the finite-difference lattice were set to the sum of the Debye-Hückel potentials.

The non polar contribution to the solvation energy ΔG_{sol}^{np} was calculated from the following equation:[43]

$$\Delta G_{sol}^{np} = \gamma SA + b \quad (4)$$

in which γ = 0.00542 kcal/Å^2, b = 0.92 kcal/mol, and SA is the solvent-accessible surface estimated using a modified version of the so-called Connolly algorithm[45, 46], based on semi-empirical molecular orbital calculations[29].

To complete the estimate of the free energy of binding, we should also calculate the entropy components arising from the solute degrees of freedom. Given that our goal was a qualitative comparison of ΔG_{bind} for the different inhibitors, we assumed that the entropies were similar in magnitude for the close-structured compounds. This assumption seems reasonable, given our previous experience[34] and Kuhn and Kollman's calculated values of $T\Delta S$ for various ligands binding to avidin.[47] Also, the results of these two authors show that this term tends to be larger in magnitude the larger the ligand. Since the van der Waals surface areas for all the compounds **2a-l** - estimated using the same method employed for the evaluation of the corresponding SA described above[29] - is confined within the range of about 50 Å^2, we concluded that the assumption of Kuhn and Kollman could be safely applied to our calculations. Accordingly, the time-consuming entropy calculations were not carried out.

Acknowledgements

The Authors would like to thank Dr. M. Cebulec for the microanalyses. This research was carried out with the financial support of the Italian M.U.R.S.T. (60%). S.P. would like to personally thank Steve Kelly (Institute of Biological Sciences, University of Wales, Aberystwyth, U.K.) for kindly providing the 3D model of 14DM.

References and Notes

1. Fioravanti, R.; Biava, M.; Porretta, G. C.; Artico, M.; Lampis, G.; Deidda, D.; Pompei, R. *Med. Chem. Res*. **1997**, *7*, 87.
2. Biava, M.; Fioravanti, R.; Porretta, G. C.; Sleiter, G.; Ettorre, A.; Deidda, D.; Lampis, G.; Pompei, R. *Med. Chem. Res*. **1997**, *7*, 228.
3. Mamolo, M. G.; Vio, L.; Banfi, E.; Cinco, M. *Eur. J. Med. Chem.* **1986**, *21*, 467.
4. Banfi, E.; Mamolo, M. G.; Vio, L.; Cinco, M.; Fabris, C.; Predominato, M. *J. Chemother.* **1991**, *3*, 66.
5. Mamolo, M. G.; Vio, L.; Banfi, E.; Predominato, M.; Fabris, C.; Asaro, F. *Il Farmaco* **1992**, *47,* 1055.

6. Banfi, E.; Mamolo, M. G.; Vio, L.; Predominato, M. *J. Chemother.* **1993**, *5*, 164.
7. Mamolo, M. G.; Vio, L.; Banfi, E. *Il Farmaco* **1996**, *51*, 65.
8. Mamolo, M. G.; Falagiani, V.; Vio, L.; Banfi, E. *Il Farmaco* **1999**, *54*, 761.
9. Banfi, E.; Mamolo, M. G.; Zampieri, D.; Vio, L.; Monti-Bragadin, C. *J. Antimicrob. Chemother.* **2001**, *48*, 705.
10. Raag, R.; Li, H.; Jones, B. C.; Poulos, T. L. *Biochemistry* **1993**, *32*, 4571.
11. Novotny, J.; Sharp, K. A. *Progr. Biophys. Mol. Biol.* **1992**, *58*, 203.
12. Misra, V. K.; Sharp K. A.; Friedman R. A.; Honing B. H. *J. Mol. Biol.* **1994**, *238*, 245.
13. Misra, V. K.; Hecth, J. L.; Sharp, K. A.; Friedman, R. A.; Honing, B. H. *J. Mol. Biol.* **1994**, *238*, 264.
14. Sharp, K. A *Biophys. Chem.* **1996**, *61*, 37.
15. Shen, J.; Wendoloski, J. *J. Comput. Chem.* **1996**, *17*, 350.
16. Novotny, J.; Bruccoleri, R. E.; Davis, M.; Sharp, K. A. *J. Mol. Biol.* **1997**, *268*, 401.
17. Bruccoleri, R. E.; Novotny, J.; Davis, M. E. *J. Comput. Chem.* **1997**, *18*, 268.
18. Godefroi, E. F.; Heeres, J.; van Cutsem, J.; Janssens, P. A. J. *J. Med. Chem.* **1969**, *12*, 781.
19. McClatchy, J. K. In *Antibiotics in Laboratory Medicine*; Lorian, V. Ed.; William & Wilkins: Baltimore, 1986, pp 181-222.
20. Boscott, P. A.; Grant, G. H. *J. Mol. Graph.* **1994**, *12*, 185.
21. Lamb, D. C.; Kelly, D. E.; Baldwin, B. C.; Gozzo, F.; Boscott, P.; Richards, W. G.; Kelly, S. L. *FEMS Microbiol. Lett.* **1997**, *149*, 25.
22. Case, D. A.; Pearlman, D. A.; Caldwell, J. W.; Cheatham III, T. E.; Ross, W. S.; Simmerling, C. L.; Darden, T. A.; Merz, K. M.; Stanton, R.V.; Cheng, A. L.; Vincent, J. J.; Crowley, M.; Tsui, V.; Radmer, R. J.; Duan, Y.; Pitera, J.; Massova, I.; Seibel, G. L.; Singh, U. C.; Weiner, P. K.; Kollman, P. A. AMBER 6, **1999**, University of California, San Francisco, U.S.A.
23. Pearlman, D. A.; Case, D. A.; Caldwell, J. W.; Ross, W. S.; Cheatham III, T. E.; DeBolt, S.; Ferguson, D.; Seibel, G. L.; Kollman, P. A. *Comp. Phys. Commun.* **1995**, *91*, 1.
24. Cornell, W. D.; Cieplak, P.; Bayly, C. I.; Gould, I. R.; Merz Jr., K. M.; Ferguson, D. M.; Spellmeyer, D. C.; Fox, T.; Caldwell, J. W.; Kollman, P. A. *J. Am. Chem. Soc.* **1995**, *117*, 5179.
25. Jayaram, B.; Sprous, D.; Beveridge, D. L. *J. Phys. Chem. B* **1998**, *102*, 9571.
26. Weiser, J.; Shenkin, P. S.; Still, W. C. *J. Comp. Chem.* **1999**, *20*, 217.
27. Materials Studio Program Package (v. 2.2), Accelrys Inc., San Diego, CA, USA.
28. Discover Program Package, as implemented in ref. g.
29. Fermeglia, M.; Pricl, S. *AIChE J*. **1999**, *45*, 2619.
30. Bayly, C. I.; Cieplak, P.; Cornell, W. D.; Kollman, P. A. *J. Phys. Chem.* **1993**, *97*, 10269.
31. Cornell, W. D.; Cieplak, P.; Bayly, C. I.; Kollman, P. A. *J. Am. Chem. Soc.* **1993**, *115*, 9620.
32. Cieplak, P.; Cornell, W. D.; Bayly, C. I.; Kollman, P. A. *J. Comp. Chem.* **1995**, *16*, 1357.
33. Hehre, W. J.; Radom, L.; van Schleyer, P. R.; Pople, J. A. *Ab Initio Molecular Orbital Theory*; New York: John Wiley & Sons, 1986.

34. Felluga, F.; Fermeglia, M.; Ferrone, M.; Pitacco, G.; Pricl, S.; Valentin, E. *Tetrahedron: Asymmetry* **2002**, *13*, 475.
35. Morris, G. M.; Goodsell, D. S.; Halliday, R. S.; Huey, R.; Hart, W. E.; Belew, R. K.; Olson, A. J. *J. Comput. Chem.* **1998**, *19*, 1639.
36. Mehler, E. L.; Solmajer, T. *Protein Eng.* **1991**, *4*, 903.
37. Jorgensen, W. L.; Chandrasekhar, J.; Madura, J. D.; Impey, R. W.; Klein, M. L. *J. Comput. Phys.* **1983**, *79*, 926.
38. Berendsen, H. J. C.; Postma, J. P. M.; van Gunsteren, W. F.; DiNola, A.; Haak, J. R. *J. Comput. Phys.* **1984**, *81*, 3684.
39. Ryckaert, J. P.; Ciccotti, G.; Berendsen, H. J. C. *J. Comput. Phys.* **1977**, *23*, 327.
40. Srinivasan, J.; Cheatham III, T. E.; Cieplak, P.; Kollman, P. A.; Case, D. A. *J. Am. Chem. Soc.* **1998**, *120*, 9401.
41. Sharp, K. A.; Honig, B. H. *Annu. Rev. Biophys. Chem.* **1990**, *19*, 301.
42. Chong, L. T.; Duan, Y.; Wang, L.; Massova, I.; Kollman, P. A. *Proc. Natl. Acad. Sci.* **1999**, *96*, 14330.
43. Sitkoff, D.; Sharp, K. A.; Honig, B. H. *J. Phys. Chem.* **1994**, *98*, 1978.
44. Gilson, M. K.; Sharp, K. A.; Honig, B. H. *J. Comput. Chem.* **1987**, *9*, 327.
45. Connolly, M. L. *Science* **1983**, *221*, 709.
46. Connolly, M. L. *J. Am. Chem. Soc.* **1985**, *107*, 1118.
47. Kuhn, B.; Kollman, P. A. *J. Med. Chem.* **2000**, *43*, 3786.